BMC Cancer

RESEARCH

Open Access

Spermine accumulation via spermine synthase promotes tumor cell proliferation in head and neck squamous cell carcinoma

Xi Chen[1,2,3,4†], Fei Song[5†], Peng Xiao[1,2,3,4†], Yisong Yao[1,2,3,4], Dongxian Li[1,2,3,4], Yuhui Fang[1,2,3,4,6], Shijun Lv[1,2,3,4], Yakui Mou[1,2,3,4*], Yumei Li[1,2,3,4*] and Xicheng Song[1,2,3,4*]

Abstract

Background Head and neck squamous cell carcinoma (HNSCC) is among the most aggressive malignancies, underscoring the need for early diagnosis to improve patient outcomes. Tumor-derived exosomes, which can be non-invasively obtained and reflect the metabolic state of tumors in real-time, are under increasing investigation for their diagnostic potential. Herein we analyzed metabolite differences in exosomes, serum, and tissues from patients with HNSCC to identify potential diagnostic biomarkers of clinical relevance.

Methods Non-targeted metabolomics based on liquid chromatography–mass spectrometry was employed to quantify metabolites in exosome, serum, and tissue samples from 11 patients with HNSCC and six patients without cancer. The metabolic profiles of HNSCC were analyzed through univariate and multivariate statistical methods, differential metabolite analysis, and pathway enrichment analysis.

Results We identified three differential metabolites in exosomes, 45 in serum, and 33 in tissues. Notably, patients with HNSCC exhibited significant disruptions in protein and amino acid metabolism. Spermine was exclusively detected in exosomes and tissues from patients with HNSCC. We hypothesize that spermine is extracellularly secreted by malignant cells via exosomes and subsequently enters the bloodstream. Moreover, spermine synthase was highly expressed in HNSCC tissues. Knocking down spermine synthase markedly impaired HNSCC cell proliferation and migration.

Conclusions This study provides a preliminarily characterization of the metabolic profile of HNSCC and highlights spermine and its synthetic pathways as potential diagnostic and therapeutic targets. Future studies are warranted to elucidate the mechanism of action of spermine in HNSCC and explore its utility in early diagnosis and therapeutic development.

Keywords HNSCC, Spermine synthase, Metabolomics, Liquid chromatography–mass spectrometry, Diagnostic biomarkers, Tumor metabolism, Amino acid metabolism

†Xi Chen, Fei Song and Peng Xiao contributed equally to the work.

*Correspondence:
Yakui Mou
muykmd@126.com
Yumei Li
myheart1263@163.com
Xicheng Song
drxchsong@163.com
Full list of author information is available at the end of the article

Background

Head and neck cancer is among the most prevalent malignancies, with > 870,000 new cases and > 440,000 deaths reported globally in 2020 [1]. As high as 90% of these cases present with head and neck squamous cell carcinoma (HNSCC), a highly heterogeneous and aggressive disease with a strong tendency toward recurrence and metastasis. Patients diagnosed at an early stage have a high cure rate; however, early clinical manifestations are often subtle, and most patients thus present with advanced HNSCC at the time of diagnosis [2, 3]. This highlights the urgent need for novel early detection methods. Recent studies have identified several biomarkers in blood and saliva, such as VEGF-A, miRNA-21, miRNA-184, and asparagine, which show promise for diagnosing HNSCC [4–6]. However, further investigations are required to confirm their clinical value and underlying mechanisms.

Exosomes, which are widely distributed in various body fluids, reflect the biological characteristics of their originating cells [7]. By transporting bioactive molecules (e.g., DNA, RNA, and amino acids), they contribute to creating a tumor microenvironment conducive to tumor invasion and metastasis [7, 8]. Compared with biomarkers in serum and saliva, exosome-based biomarkers demonstrate superior performance [9, 10]. The search for tumor biomarkers in exosomes has been conducted in several cancer types, with various miRNAs, long noncoding RNAs, and proteins showing potential diagnostic value [11–14].

During cancer progression, cancer cells undergo metabolic reprogramming to meet the demands of rapid growth and survival. Glycolysis, pentose phosphate pathway, tricarboxylic acid cycle, and glutamine metabolism are reportedly upregulated in patients with HNSCC. In addition, levels of various metabolites, such as lactate, gamma-aminobutyric acid, and polyamine-based metabolites, are elevated [15–19]. In comparison to the transcriptome and proteome, the metabolome is more closely linked to the biological phenotype [20]. Metabolomic analysis has been applied to diverse tumors, such as gastric cancer [21], hepatocellular carcinoma [22, 23], breast cancer [24]. and lung cancer [25]. Besides, metabolomic studies using gas chromatography–mass spectrometry and liquid chromatography–mass spectrometry (LC–MS) have identified potential diagnostic biomarkers for HNSCC [26, 27]. Exosome metabolomics, in particular, has shown promise in cancer diagnostics. For instance, Tao et al. linked specific lipid profiles in serum exosomes to pancreatic cancer progression, facilitating early diagnosis [27]. Similarly, other studies employing targeted metabolomics and machine learning have reported the identification of biomarker sets for disease prediction and screening in esophageal squamous cell carcinoma and lung cancer [28, 29].

In this study, we analyzed the metabolic signatures of cancer tissues, serum, and exosomes from patients with HNSCC using LC–MS/MS-based non-targeted metabolomics. We focused on identifying differential metabolites to recognize reliable diagnostic biomarkers for HNSCC. Our metabolomics data revealed distinct alterations between patients with HNSCC and controls, with spermine showing the highest diagnostic potential. Subsequent experiments confirmed the role of spermine synthase (SMS) in promoting tumor progression.

Methods

Patient cohort

We collected cancer tissues, adjacent normal tissues, serum, and exosomes from 11 patients with HNSCC, and control serum and exosomes from participants without cancer or inflammation related diseases at Yantai Yuhuangding Hospital. (Supplementary Table 1) Patients who had undergone preoperative radiotherapy, targeted therapy, biologic therapy, or had incomplete clinical data were excluded. All participants provided written informed consent, and the study was approved by the ethics committee of Yantai Yuhuangding Hospital. Serum samples were obtained by blood centrifugation at 3,000 rpm for 10 min at 4 °C and stored at − 80 °C until needed.

Exosome sample preparation

Exosomes were isolated using the QIAGEN exoEasy Maxi Kit, according to manufacturer instructions. Serum samples were centrifuged at 3,000 × g for 15 min at 4 °C and then mixed with XBP buffer in a 1:1 ratio. This mixture was transferred to an exoEasy spin column and centrifuged at 500 × g for 1 min at 4 °C. Subsequently, 10 mL XWP buffer was added, followed by centrifugation at 5,000 × g for 5 min. Finally, exosomes were eluted with 400 µL XE buffer and centrifuged again at 500 × g for 5 min at 4 °C.

Transmission electron microscopy

Exosomes were deposited onto a sealing membrane and covered with a copper grid. The sample was fixed by incubating the grid with 3% glutaraldehyde for 5 min. Subsequently, the grid was washed 10 times with 20 µL distilled water for 2 min each. The sample was then stained with 4% uranyl acetate for 10 min on ice, air-dried, and visualized using transmission electron microscopy.

Metabolite extraction

Add extraction solution (methanol: acetonitrile: water = 2:2:1) and 10 µL of internal standard in each

tissue sample. After homogenization at 40 Hz for 5 min, the samples were sonicated for 10 min and incubated at 20 °C for 1 h. The samples were then centrifuged at 25,000 rpm for 15 min at 4 °C, and the supernatant was collected for vacuum freeze-drying. Metabolites were resuspended in 200 µL of 10% methanol, sonicated, and centrifuged again under the same conditions. In order to provide more reliable experimental results during instrument testing, the samples are randomly ordered to reduce system errors. A quality control (QC) sample was prepared by pooling 20 µL from each sample to create a representative mixture and interspersed for every 10 samples to ensure the accuracy and precision of the analytical method throughout the study.

LC–MS/MS

Metabolite analysis was performed on a Waters 2D UPLC system coupled with a Q-Exactive mass spectrometer (Thermo Fisher Scientific). Chromatographic separation was performed on a Waters ACQUITY UPLC BEH C18 column (1.7 µm, 2.1 mm × 100 mm) maintained at 45 °C.

Detection and identification of metabolites

The mass spectrometry raw data (raw file) collected by LC–MS/MS was imported into Compound Discoverer 3.1 (Thermo Fisher Scientific, USA) for data processing, including peak extraction, retention time correction within and between groups, additive ion pooling, missing value filling, background peak labeling, and metabolite identification, and finally information on compound molecular weight, retention time, peak area, and identification results were exported. The identification of metabolites is a combined result of BGI self-built standard library, mzCloud and ChemSpider (HMDB, KEGG, LipidMaps) databases.

Differential metabolite analysis

We identified differential metabolites between the groups using multivariate statistical analyses, including principal component analysis, partial least squares discriminant analysis (PLS-DA), and orthogonal PLS-DA (OPLS-DA), as well as univariate analyses such as fold-change (FC) analysis and Student's *t*-test. The criteria for differential metabolite screening were (1) variable importance in projection score of ≥ 1 for the first two principal components in the PLS-DA model, (2) FC ≥ 1.2 or ≤ 0.83, and (3) $p < 0.05$. Differential metabolites were grouped using a hierarchical clustering algorithm. Data were $\log_2$-transformed and normalized using z-scores. Euclidean distance was applied to calculate the distance for clustering. Metabolites were annotated based on the Kyoto Encyclopedia of Genes and Genomes (KEGG) database (www.genome.jp/kegg) and the Human Metabolome Database (hmdb.ca). Differential metabolites were subjected to metabolic pathway enrichment analysis using the KEGG database.

Data visualization

A Venn diagram was constructed using an online portal (https://bioinformatics.psb.ugent.be/webtools/Venn/) to show the shared and unique metabolites between samples from tumor tissues, adjacent normal tissues, tumor and control serum and exosomes.

Expression profile and clinical features

RNA-sequencing data and clinical information were obtained from The Cancer Genome Atlas (TCGA) database (http://cancergenome.nih.gov/). Violin plots depicting SMS expression profiles and correlations with clinical features were created using Hiplot (https://hiplot.org/). The Kaplan–Meier method, accessed through Gene Expression Profiling Interactive Analysis (http://gepia.cancer-pku.cn/), was used for survival analysis.

Cell culture

The laryngeal squamous cell carcinoma cell line AMC-HN-8 was cultured in RPMI 1640 medium (Viva Cell). The hypopharyngeal carcinoma cell line FaDu was cultured in MEM-E medium (Viva Cell) supplemented with 10% fetal bovine serum (Biochannel). Both these cell lines were maintained at 37℃ in a humidified atmosphere with 5% carbon dioxide.

Small-interfering RNA (siRNA) transfection

To transient knockdown of SMS expression, sequence-specific siRNA was used. Cells were transfected with 50 nM SMS-targeting siRNA or negative control siRNA (GenePharma, Shanghai, China) using Lipofectamine 3000 (Invitrogen, CA, USA) in serum-free medium. After 6 h, the transfection mixture was replaced with fresh medium containing 10% fetal bovine serum. Cells were then incubated for 48 h before further experiments.

CCK-8 assay

Fadu cells (2×10^3) were placed in 96-well plates and cell viability was measured every 12 h. For measurement, 10 µL of CCK-8 solution was dropped into each well and incubated for 2 h. Absorbance was measured by microplate reader at 450 nm.

Colony formation assay

Cells were seeded into 6-well plates (1,000 cells/well), with the medium replaced every 48 h. After 10–14 days of incubation, colonies were fixed in 4% paraformaldehyde and stained with 0.1% crystal violet. Colony number

was counted for each treatment group across three replicate wells.

Wound healing assay

Forty-eight hours post-transfection, vertical scratches were made in cell monolayers using a 200 μL plastic filter tip. The medium was replaced with media containing 1% fetal bovine serum. Cell migration was assessed at 0, 12, and 24 h under an inverted microscope.

RNA isolation, reverse transcription, and quantitative PCR (qPCR)

Total RNA was extracted from cells using TRIzol (SparkJade) and reverse transcribed into cDNA using SPARKscript II All-in-one RT SuperMix for qPCR (With gDNA Eraser) (SparkJade). Quantitative real-time PCR (qRT-PCR) was performed using ChamQ SYBR qPCR Master Mix (Vazyme), following manufacturer instructions for cycle and temperature conditions. Gene expression was normalized using β-actin as internal controls. The following primer sequences were used: β-actin, forward 5′-TGGTGGGCATGGGTCAGAAGG-3′ and reverse 5′-ACGCAGCTCATTGTAGAAGGTGTG-3′; and SMS, forward 5′-GCTGGACCTTCAGAGTTATGATGG-3′ and reverse 5′-GGCTCCTCCTCGCACTATGG-3′.

Western blotting

Cellular and exosomal proteins were extracted using RIPA lysis buffer (SparkJade) with 1% phenylmethanesulfonyl fluoride (SparkJade). Proteins were separated by 10% sodium dodecyl sulfate–polyacrylamide gel electrophoresis at 80 V for 30 min, followed by 120 V for 60 min, and then transferred onto nitrocellulose membranes. The membranes were blocked at room temperature for 2 h, and then incubated overnight at 4 °C with primary antibodies (Sangon Biotech). Subsequently, the membranes were incubated with secondary antibodies (Sangon Biotech) at room temperature for 2 h.

Statistical analysis

Statistical analyses were performed using SPSS v27.0. Graphics were mainly generated by GraphPad Prism 9.0. Statistically significant differences were evaluated using Student's *t*-test. $p < 0.05$ indicated statistical significance.

Results

Differential metabolite analysis in HNSCC serum exosomes

We rigorously evaluated the performance of our analytical system using QC samples. Base peak chromatogram detection in the QC group demonstrated well-shaped peaks and high peak capacity in both positive and negative ion modes (Figure S1A, S1B). The spectrum overlap exhibited favorable characteristics, with minimal fluctuations in retention time and peak response intensity. Metabolites with coefficient of variation ≤ 30% of the relative peak area in the QC samples accounted for 90.47% in positive ion mode and 90.37% in negative ion mode of all detected metabolites (Figure S1C, S1D). Principal component analysis revealed clear separation between tissue, serum, exosome, and QC groups, with tight clustering of QC samples, demonstrating the stability of the analytical system and reliability of obtained data (Figure S1E, S1F).

Transmission electron microscopy was utilized to observe the morphology and structure of serum exosomes (Fig. 1A). The extracted exosomes showed a typical "teato-like" structure, with all of them exhibiting round or oval double-membraned vesicle-like structures; their diameters were normal, ranging from 30 to 150 nm. Western blotting confirmed that serum exosomes highly expressed the exosome biomarkers CD9, TSG101, and CD63 (Fig. 1B).

In HNSCC serum exosomes, 794 metabolites were detected, with 180 identified, while 767 metabolites were detected in control serum exosomes, of which 160 were identified. OPLS-DA plots (Fig. 1C) indicated a trend of separation between HNSCC and control serum exosomes ($R^2 = 0.95$, $Q^2 = -0.46$; Fig. 1D). Three metabolites showed significant expression differences (Supplementary Table 3). Phenylalanine expression was upregulated in the HNSCC group (Fig. 1E, F) [30]. Dysregulation was observed in four metabolic pathways: sulfur metabolism; protein digestion and absorption; phenylalanine, tyrosine, and tryptophan biosynthesis; and sphingomyelin biosynthesis (Fig. 1G).

Differential metabolite analysis in HNSCC tissues

In positive and negative ion modes, 4,201 metabolites were detected in HNSCC tissues, with 1,586 identifiable. In adjacent normal tissues, 2,972 metabolites were detected, of which 1,172 were identified. By applying OPLS-DA, we could observe a clear separation trend between the groups (Fig. 2A). Response permutation testing confirmed model stability and reliability ($R^2 = 0.84$, $Q^2 = -0.39$; Fig. 2B).

A heatmap was plotted, which showed distinct clustering of metabolites between cancer and adjacent normal tissues (Fig. 2C, D). A total of 33 differential metabolites were identified between the HNSCC and adjacent normal groups, of which 13 were identified as amino acids or peptides and their derivatives (Supplementary Table 3). The expression of these metabolites, such as arginine, leucine, serine, tyrosine, and various dipeptides, was predominantly upregulated in the cancer group, suggesting increased protein synthesis and degradation within tumor tissues.

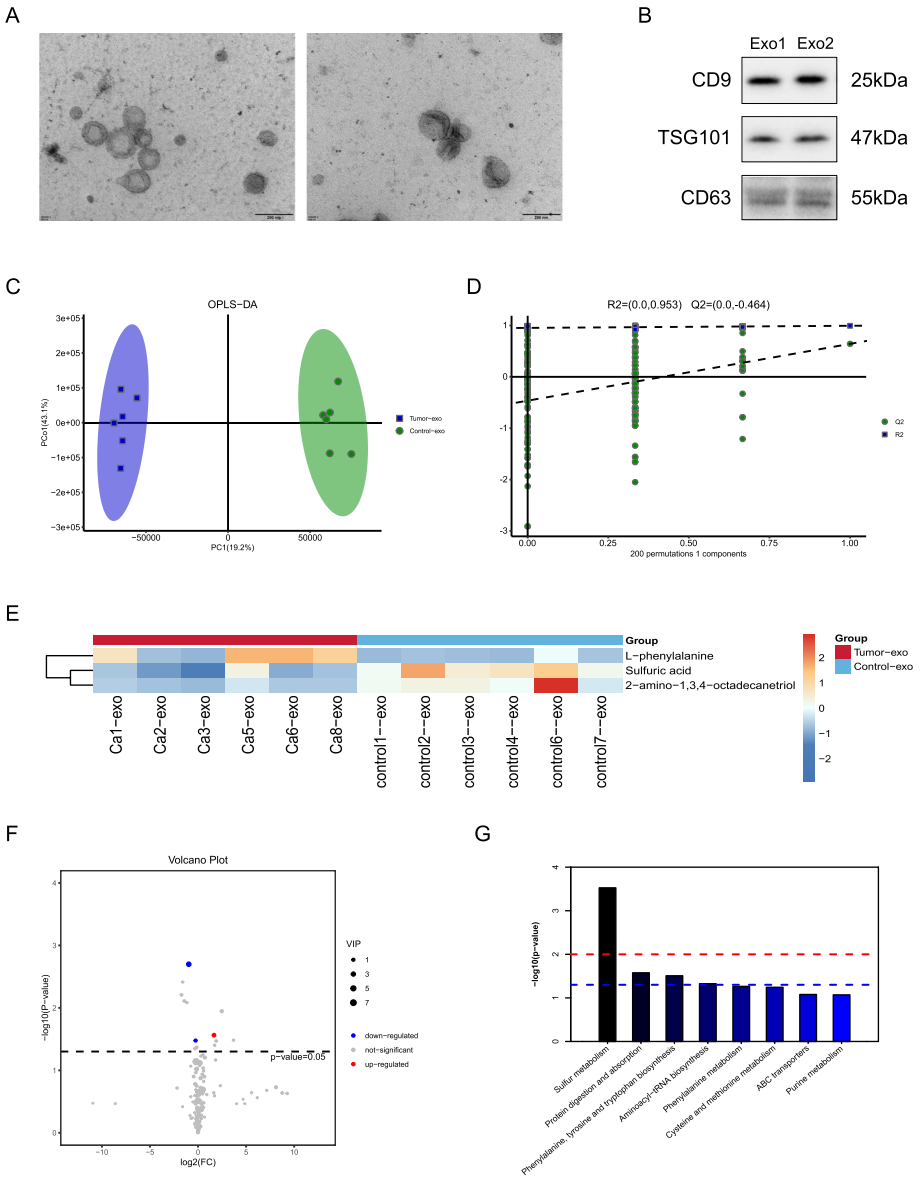

Fig. 1 Identification and comprehensive metabolomic analysis of HNSCC serum exosomes. **A** Transmission electron microscopy: exosomes exhibit a bilayer lipid-encapsulated, disc-like morphology, with diameters ranging from 30 to 150 nm (scale: 200 nm). **B** Western blotting: exosome markers (CD9, TSG101, and CD63) were found to be significantly expressed. **C** Score plot of the OPLS-DA model. **D** Response permutation testing plot for the OPLS-DA model. The two rightmost points represent the actual R^2Y and Q^2 values, while the remaining points show values obtained by random rearrangement of the samples. **E** Heatmap of clustering analysis. Each row represents a differential metabolite, and each column represents a sample. Colors correspond to expression levels, with blue indicating low and red indicating high expression. **F** Volcano plot. Blue indicates downregulated differential metabolites (labeled blue), red indicates upregulated differential metabolites (labeled red), and gray indicates no significant change. **G** KEGG pathway analysis of differential metabolites

Pathway enrichment analysis of the top 20 metabolites, performed using the KEGG database (Fig. 2E), revealed a close association between arginine biosynthesis and HNSCC. Elevated levels of argininosuccinate synthase, a key enzyme in de novo arginine synthesis, have been lined to poor prognosis in patients with cancer [31, 32]. These metabolic alterations likely reflect the rapid proliferation and altered energetic demands of cancer cells [33].

Differential metabolite analysis in HNSCC serum samples

A total of 3,906 metabolites were detected in HNSCC serum samples, with 1,310 metabolites identified, compared to 3,210 metabolites detected in control

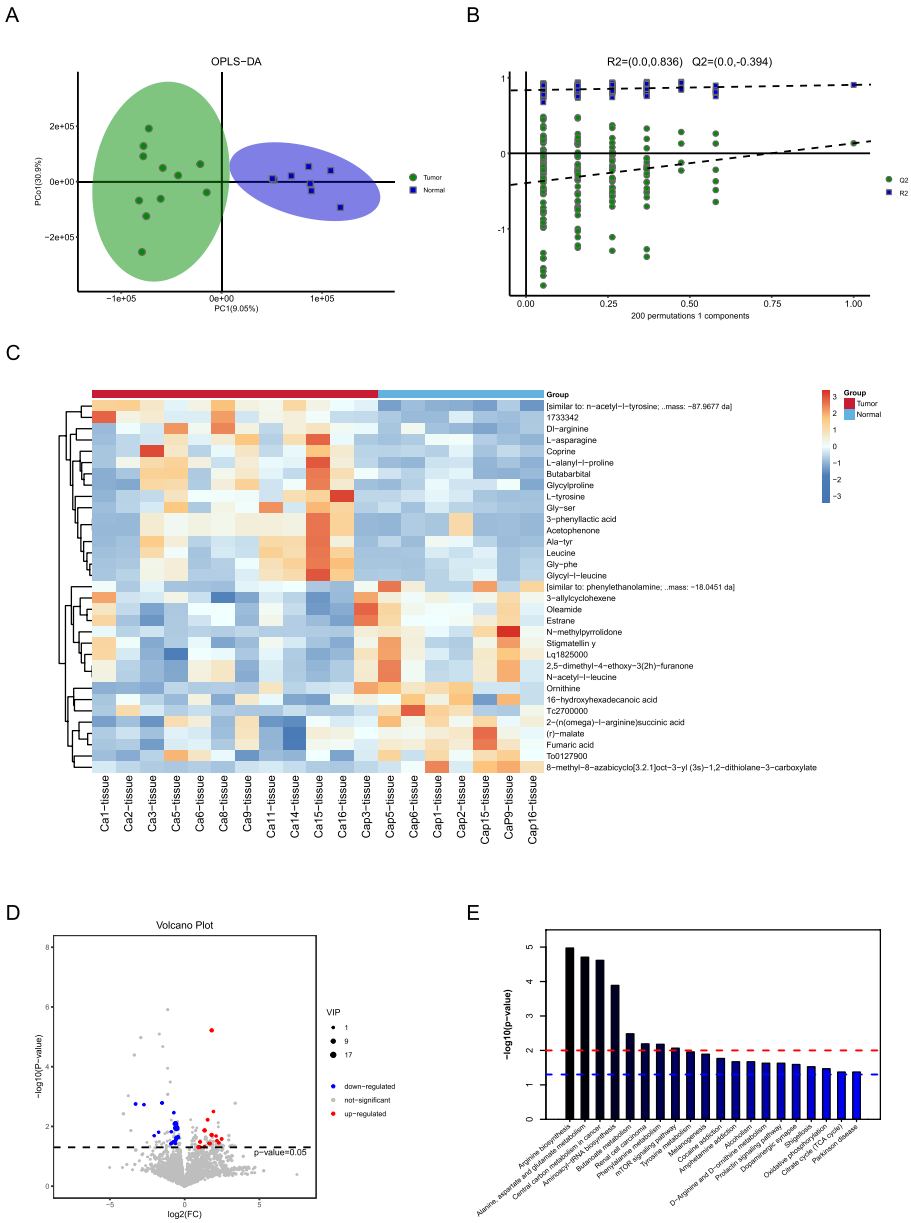

Fig. 2 Comprehensive metabolomic analysis of HNSCC tissues. **A** Score plot of the OPLS-DA model. **B** Response permutation testing plot for the OPLS-DA model. The two rightmost points represent the actual R^2Y and Q^2 values of the model, while the remaining points show values obtained by random rearrangement of the samples. **C** Heatmap of clustering analysis. Each row represents a differential metabolite, and each column represents a sample. Colors correspond to expression levels, with blue indicating low and red indicating high expression. **D** Volcano plot. Blue indicates downregulated differential metabolites (labeled blue), red indicates upregulated differential metabolites (labeled red), and gray indicates no significant change. **E** KEGG pathway analysis of differential metabolites

serum samples, of which 1,091 were identified. OPLS-DA plots (Fig. 3A) demonstrated a clear separation between the groups ($R^2 = 0.98$, $Q^2 = -0.35$; Fig. 3B). A heatmap and volcano plot were plotted (Fig. 3C, D), resulting in the identification of 45 differential metabolites, of which six were up- and 39 were downregulated in HNSCC (Supplementary Table 3). Notably, citrulline and acetylcarnitine serum levels were elevated in HNSCC serum. Pathway enrichment analysis of the top 20 differential metabolites revealed changes in several crucial metabolic pathways in HNSCC, including choline metabolism, glycerophospholipid metabolism, cholinergic synapses, and insulin resistance (Fig. 3E).

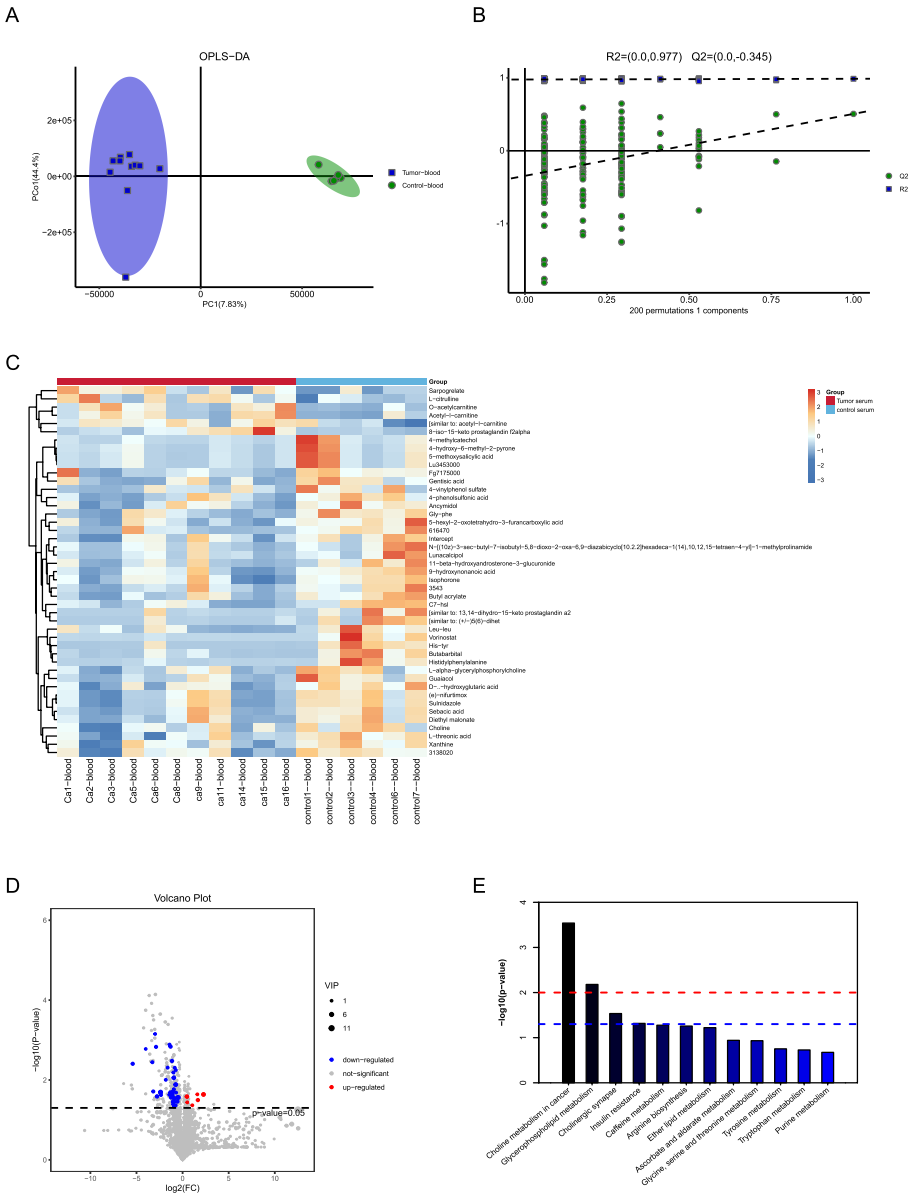

Fig. 3 Comprehensive metabolomic analysis of HNSCC serum samples. **A** Score plot of the OPLS-DA model. **B** Response permutation testing plot for the OPLS-DA model. The two rightmost points represent the actual R^2Y and Q^2 values, while the remaining points show values obtained by random rearrangement of the samples. **C** Heatmap of clustering analysis. Each row represents a differential metabolite, and each column represents a sample. Colors correspond to expression levels, with blue indicating low and red indicating high expression. **D** Volcano plot. Blue indicates downregulated differential metabolites (labeled blue), red indicates upregulated differential metabolites (labeled red), and gray indicates no significant change. **E** KEGG pathway analysis of differential metabolites

Spermine as a potential biomarker for HNSCC

A Venn diagram visualizing shared and unique metabolites among the groups (Fig. 4A, Supplementary Table 2) revealed that of the 175 HNSCC exosome metabolites, 125 were also present in HNSCC tissue metabolites. In contrast, serum samples contained a higher proportion of unique metabolites, likely reflecting systemic versus local tissue metabolite differences. Spermine was detected only in HNSCC exosomes and tissues but not in adjacent normal tissues, exosomes, serum, or HNSCC serum, indicating that spermine may be secreted from cancer cells into exosomes and subsequently enter the bloodstream. SMS, a key regulatory enzyme in spermine synthesis, showed significantly higher expression in HNSCC compared to controls in TCGA dataset (Fig. 4B). Further investigation into the clinical significance of

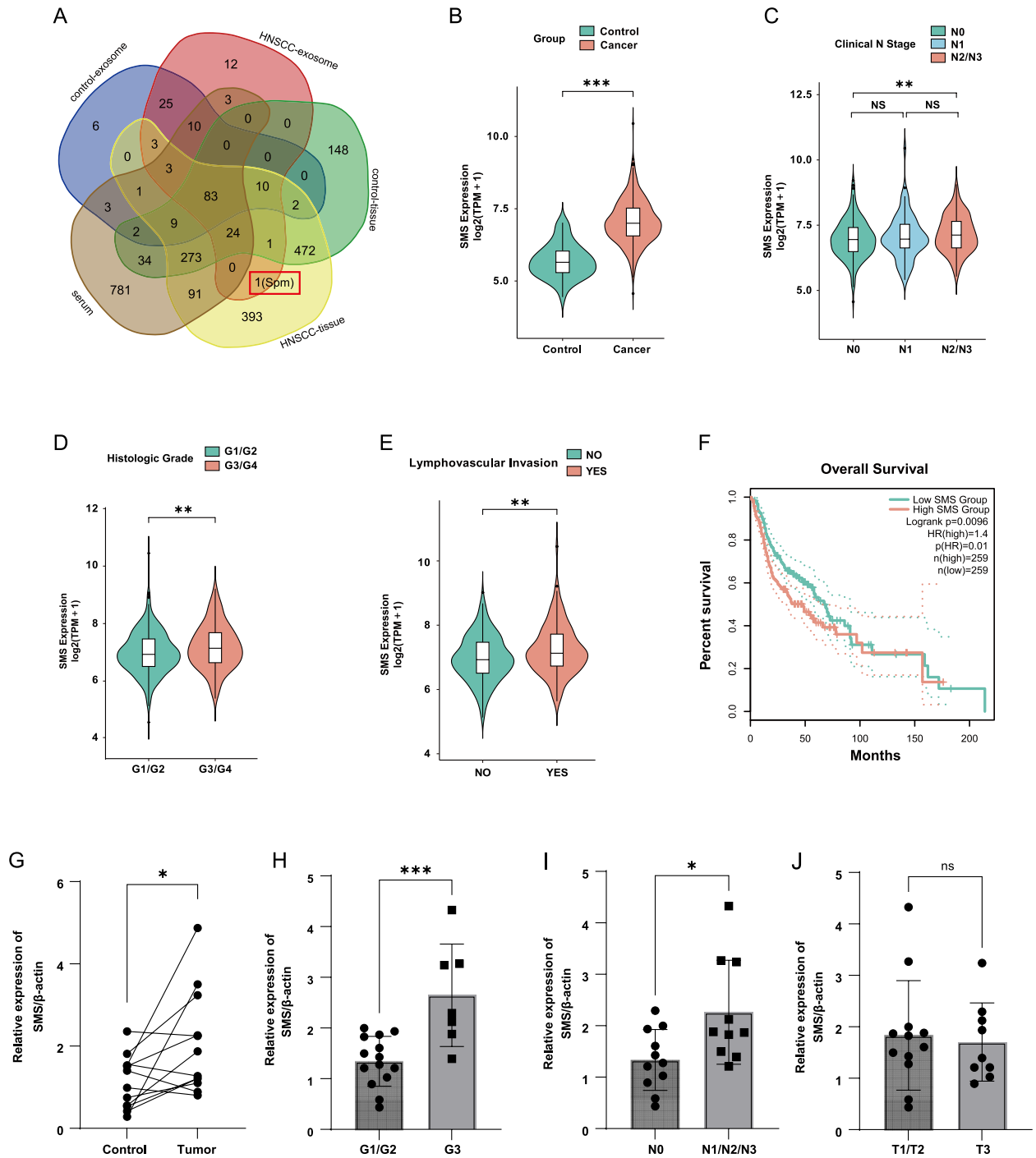

Fig. 4 Expression of SMS in patients with HNSCC and its clinical relevance. **A** Venn diagram showing metabolite overlap between the groups. Analysis from TCGA database (**B**) showing differential SMS expression between HNSCC and normal tissues. **C** Changes in SMS expression across different clinical N stages and (**D**) histological grades based on data from TCGA database. **E** Association of SMS expression with lymphovascular invasion from TCGA database. **F** Kaplan–Meier analysis illustrating the effects of SMS expression on overall survival. The group cutoff is determined by quartile. **G** SMS expression levels in 12 HNSCC tissue and paired adjacent normal tissues. **H**-**J** Changes in SMS expression across different clinical N stages (**H**), histological grades (**I**) and T stage (**J**) ($n = 21$)

SMS in HNSCC revealed that elevated SMS expression was associated with advanced clinical N stage (Fig. 4C), higher histological grades (Fig. 4D), and lymphovascular invasion (Fig. 4E), suggestive of a relationship between increased expression of SMS and aggressive progression of HNSCC. Kaplan–Meier survival analysis indicated that high SMS expression correlated with lower overall survival in patients with HNSCC (Fig. 4F). We assessed the expression levels of SMS in human HNSCC and adjacent normal tissues. Our results revealed that SMS was highly expressed in tumor tissues (Fig. 4G). Patients with elevated SMS expression were more likely to have higher histological grades (Fig. 4H) and a greater probability of lymph node metastasis (Fig. 4I). However, no significant differences were observed in T stage (Fig. 4J). These findings are consistent with the analysis of data from the TCGA database.

SMS knockdown inhibits HNSCC growth

To investigate the role of SMS in HNSCC, we used siRNA to knockdown SMS in FaDu and AMC-HN-8 cells, with knockdown efficiency confirmed at both the RNA and protein levels (Fig. 5A, B, Supplementary Fig. 2A, B). SMS knockdown markedly inhibited cell proliferation and colony formation (Fig. 5C, D). Moreover, wound healing assays demonstrated that SMS expression downregulation impaired cell migration (Fig. 5E). These findings suggest that SMS promotes HNSCC progression by modulating cellular proliferation and migration.

Discussion

The increasing prevalence of HNSCC necessitates the adoption of more efficient diagnostic methods in clinical practice [34]. Liquid biopsy presents a more cost-effective and less invasive alternative to traditional tissue biopsy, enabling real-time monitoring of cancer status through serial testing. Exosomes offer significant advantages for clinical diagnosis due to their enhanced stability compared to other liquid biopsy types. They contain a diverse array of biomolecules, including proteins, miRNAs, long non-coding RNAs, circular RNAs, mitochondrial DNA, chromosomal DNA, lipids, and small molecule metabolites [35, 36]. The great promise of exosomes as biomarkers in liquid biopsy has been well-established. A variety of differential metabolites were detected in the exosomes of tumor patients compared to normal controls [37–39], which was verified to be used as tumor predictors [40, 41]. Additionally, several metabolites associated with tumor progression have been identified through the analysis of exosomes from patients at various stages of disease progression [41, 42]. At present, exosomes were also approved for the diagnosis of lung and prostate cancers in clinical [43, 44]. Considering the importance of metabolic reprogramming in cancer occurrence and development, we analyzed metabolites from serum exosomes, serum, and tumor tissues to enhance the metabolic profiling of HNSCC. In addition, we propose that spermine within exosomes may serve as a potential biomarker for diagnosis and found that SMS promotes tumor cell proliferation.

Our analysis revealed elevated levels of specific amino acids in HNSCC tissues, including leucine, arginine, and asparagine. Asparagine participates in multiple nutrient metabolism pathways through the mTORC1 signaling cascade; moreover, it plays a critical role in cancer cell development [45, 46]. Furthermore, the association between cancer progression and arginine is well-established [47, 48], while polyamines, which are metabolites derived from arginine, are essential for maintaining genomic stability [49, 50]. Using isotope tracing, Carrer et al. identified leucine as a major source of acetyl-CoA, a central metabolite in biosynthetic processes essential for cell proliferation, including fatty acid and cholesterol synthesis [51]. High levels of various dipeptides, such as Gly-Pro, Ala-Tyr, Ala-Pro, Gly-Ser, Gly-Leu, and Gly-Phe, are reportedly present in tumor tissues. Previous research suggests that dipeptides could have diagnostic utility. In a study involving 3,482 participants, researchers employed metabolomics and machine learning techniques to identify Glu-Leu and tyrosine as early diagnostic biomarkers for colorectal cancer, achieving a diagnostic accuracy of 92.38% [52]. Hershberger et al. found that Gly-Pro, while not significantly elevated in cancer, was able to enhance the diagnostic performance of machine learning models when combined with other metabolites [53].

Serum exosomes from patients with cancer exhibited increased levels of phenylalanine, consistent with the findings of a previous study utilizing nuclear magnetic resonance-based metabolic profiling of HNSCC tissues [54]. This phenomenon may arise from dysfunctional phenylalanine hydroxylase activity in inflammatory or malignant conditions. Phenylalanine hydroxylase catalyzes the conversion of phenylalanine to tyrosine, and reduced enzymatic activity leads to phenylalanine accumulation [55, 56]. Jobard et al. identified phenylalanine as a component in a model differentiating between localized early-stage disease and advanced metastatic breast cancer through nuclear magnetic resonance-based metabolic profiling [57]. Phenylalanine metabolism and its derivatives were the most significantly enriched pathways identified in an untargeted metabolomics analysis of non-small cell lung cancer [58].

Alterations in protein and amino acid metabolism were observed in cancer tissues and exosomes, with a notable enrichment of aminoacyl-tRNA biosynthesis in both the groups. Several metabolites exhibited similar trends

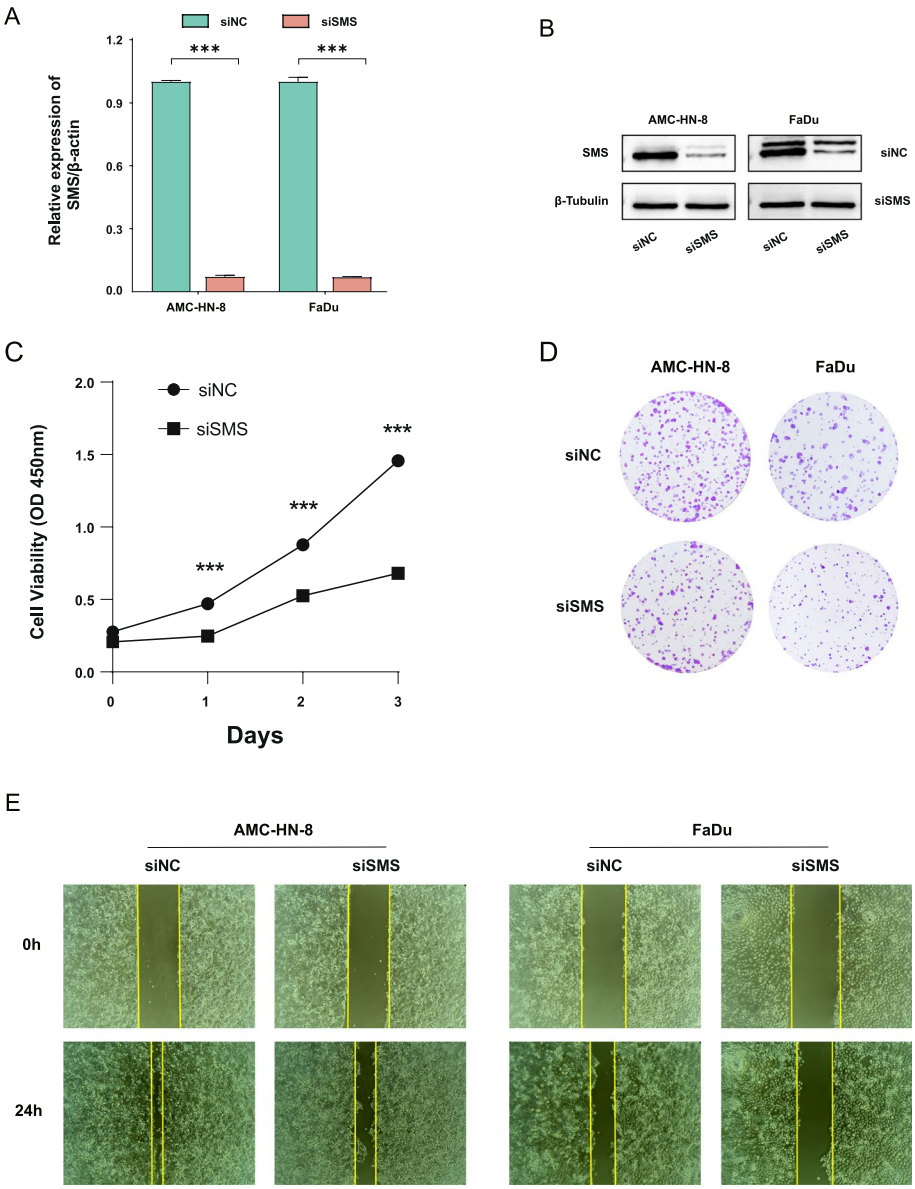

Fig. 5 SMS knockdown promotes HNSCC cell proliferation and migration. Real-time PCR (**A**) and Western blot assays (**B**) confirmed the efficiency of SMS knockdown in FaDu and AMC-HN-8 cells ($n=3$ for each). **C**, **D** Effects of SMS knockdown on cell proliferation were evaluated using CCK-8 assays (**C**) and colony formation assays (**D**) ($n=3$). **E** Effects of SMS knockdown on cell migration were assessed using wound healing assays ($n=3$). Statistical significance is represented as $^{*}p<0.05$, $^{**}p<0.01$, $^{***}p<0.001$, and $^{****}p<0.0001$

across these groups, indicating that exosomes accurately reflect the metabolic status of tumor tissues. However, aberrant lipid metabolism was predominant in serum samples, with a marked increase in acetylcarnitine levels in the cancer group. Acetylcarnitine plays a crucial role in lipid metabolism by facilitating the β-oxidation of fatty acids, thereby releasing energy [59, 60].

Variations in serum metabolic profiles are more complex than those in tissues and exosomes, reflecting the role of blood as a transport medium. This complexity also suggests that tumors influence the metabolic processes of other organs, potentially impacting serum metabolite levels.

Spermine, a small molecular compound produced through SMS-catalyzed aminopropyl transfer reactions, is crucial for normal cell growth and function [61–63]. Elevated spermine levels are frequently observed in cancer, indicative of a potential association between cancer progression and spermine biosynthesis and catabolism [63, 64].

Recent research has highlighted the roles of spermine and SMS in tumor biology. AI-Habsi et al. demonstrated that spermidine enhances antitumor immunity by activating mitochondrial trifunctional protein; however, spermidine can also bind to this protein, inhibiting this effect [65]. Spermine is crucial for tumor progression. It is reported that spermine promotes intestinal epithelial repair by accelerating Rac1/PLC-γ1 signalling-mediated cell proliferation and migration [66]. Further, the simultaneous inhibition of SMS and MYC signaling pathways can yield synergistic antitumor effects [67]. In pancreatic cancer, the METTL3–IGF2BP3 axis regulates the N6-methyladenosine modification of SMS, modulating AKT phosphorylation and activating epithelial–mesenchymal transition, thereby promoting tumor progression and migration [68]. Notably, spermine levels tend to decrease in prostate tumors [69]. In castration-resistant prostate cancer, spermine has been shown to influence epigenetic processes and inhibit androgen receptor-related pathways by targeting and inhibiting spermidine methyltransferase (PRMT1), resulting in antitumor effects [70]. This discrepancy may be attributed to the naturally high spermine levels in prostate epithelial tissue [71]. Spermine also regulates immunity. In hepatocellular carcinoma, spermine reprograms tumor-associated macrophages through activation of the PI3K-Akt-mTOR-S6K signaling pathway, promoting their polarization toward the M2 phenotype [72]. Spermine binds to JAK1, impairing the interaction between JAK1 and cytokine receptors, thereby broadly suppressing JAK1-mediated activation of downstream signaling pathways, including those of IFN-I, IFN-II, IL-6, and IL-2 [73]. In addition, spermine reportedly inhibits type I interferon responses, which are vital for the functionality of antigen-presenting cells in tumor immunity [74].

The previous study identified SMS as a potential prognostic biomarker through bioinformatics analysis [75], which supported our results. In addition, our study showed that the expression level of SMS was related to N stages, histological grades, lymphovascular invasion and prognosis. We verified the expression differences of SMS in HNSCC and adjacent normal tissue by qPCR, and we found that the knockdown of SMS impaired the progression of HNSCC through CCK8, colony assay, and would healing assay.

This study has several limitations. Although we detected several metabolites, some lacked compound identifiers. Our goal is to detect compounds as comprehensively as possible and expand our metabolite database. Non-targeted metabolomics has limitations in detecting dipeptides; thus, further studies could benefit from employing targeted assays [76]. The primary challenge of all liquid biopsy approaches remains the "noise" or interference from normal cells. Most exosomes in liquid biopsies are derived from normal cells. Future investigations should utilize enrichment strategies based on surface markers to address this issue and enhance diagnostic specificity and sensitivity [35, 77–79]. Besides, we acknowledge the limitations in making causal inferences from comparative groups in experimental designs that lack follow-up. Future studies should aim to include a more homogeneous age range and collect additional data, including anthropometric parameters, genetic profiles, and risk factors associated with HNSCC. Factors critical to improving treatment options and enhancing patient quality of life, such as recurrence and patient survival, should also be prioritized.

In summary, we employed high-throughput, non-targeted metabolomics techniques based on LC–MS/MS to delineate the metabolic patterns of patients with HNSCC and to explore potential diagnostic biomarkers in exosomes. Our findings complement existing research on the genomics and proteomics of HNSCC.

Abbreviations

HNSCC	Head and neck squamous cell carcinoma
LC–MS	Liquid chromatography–mass spectrometry
SMS	Spermine synthase
PLS-DA	Partial least squares discriminant analysis
OPLS-DA	Orthogonal PLS-DA
FC	Fold-change
KEGG	Kyoto Encyclopedia of Genes and Genomes
TCGA	The Cancer Genome Atlas
qPCR	Quantitative PCR
qRT-PCR	Quantitative real-time PCR
siRNA	Small-interfering RNA

Supplementary Information

The online version contains supplementary material available at https://doi.org/10.1186/s12885-025-13820-x.

Supplementary Material 1.

Acknowledgements
Not applicable.

Authors' contributions
X.C. and F.S. designed the study; Y.Y., D.L., Y.F. and S.L. collected samples; X.C. and F.S. performed the experiments; Y.Y. and Y.F. performed the data analysis; X.C. and P.X. wrote the manuscript; Y.M. and Y.L. revised the manuscript; X.S. supported the funding for this study. All authors read and approved the final manuscript.

Funding
This work was supported by the Taishan Scholar Project (No.ts20190991), the Key R&D Project of Shandong Province (2022CXPT023) , Shandong Medical Association clinical Research Fund-Qilu special fund YXH2022ZX02185, and High-end Talent Introduction and Cultivation under Yantai City's "Double Hundred Program"

Data availability
The datasets used in this study were obtained from The Cancer Genome Atlas (TCGA) database, which is publicly accessible at https://portal.gdc.cancer.gov/. Data analyses were performed using the Hiplot (https://hiplot.com.cn) and GEPIA (http://gepia.cancer-pku.cn) platforms, and the results can be

reproduced via these platforms. The original contributions presented in the study are included in the article/ supplementary material. Further inquiries can be directed to the corresponding authors.

Declarations

Ethics approval and consent to participate
Our study was approved by 'Ethics Committee of YanTai Yuhuangding Hospital' (approval no.: 2024–659). This study was conducted in accordance with the Declaration of Helsinki.

Consent for publication
Not applicable.

Competing interests
The authors declare no competing interests.

Author details
[1]Department of Otorhinolaryngology, Head and Neck Surgery, Yantai Yuhuangding Hospital, Qingdao University, Yantai, Shandong 264000, China. [2]Shandong Provincial Key Laboratory of Neuroimmune Interaction and Regulation, Yantai, Shandong 264000, China. [3]Shandong Provincial Clinical Research Center for Otorhinolaryngologic Diseases, Yantai, Shandong 264000, China. [4]Yantai Key Laboratory of Otorhinolaryngologic Diseases, Yantai, Shandong 264000, China. [5]Ludong University, Yantai, Shandong 264025, China. [6]The 2nd Medical College of Binzhou Medical University, Yantai, Shandong 264000, China.

Received: 4 December 2024 Accepted: 26 February 2025
Published online: 05 March 2025

References

1. Sung H, Ferlay J, Siegel RL, Laversanne M, Soerjomataram I, Jemal A, et al. Global Cancer Statistics 2020: GLOBOCAN Estimates of Incidence and Mortality Worldwide for 36 Cancers in 185 Countries. CA Cancer J Clin. 2021;71(3):209–49.
2. Mesia R, Iglesias L, Lambea J, Martínez-Trufero J, Soria A, Taberna M, et al. SEOM clinical guidelines for the treatment of head and neck cancer (2020). Clin Transl Oncol. 2021;23(5):913–21.
3. Network CGA. Comprehensive genomic characterization of head and neck squamous cell carcinomas. Nature. 2015;517(7536):576–82.
4. Edirisinghe ST, Weerasekera M, De Silva DK, Devmini MT, Pathmaperuma S, Wijesinghe GK, et al. Vascular Endothelial Growth Factor A (VEGF-A) and Vascular Endothelial Growth Factor Receptor 2 (VEGFR-2) as Potential Biomarkers for Oral Squamous Cell Carcinoma: A Sri Lankan Study. Asian Pac J Cancer Prev. 2023;24(1):267–74.
5. Garg A, Urs AB, Koner BC, Augustine J, Guru SA. Evaluation of Diagnostic Significance of Salivary miRNA-184 and miRNA-21 in Oral Squamous Cell Carcinoma and Oral Potentially Malignant Disorders. Head Neck Pathol. 2023;17(4):961–8.
6. Hu S, Zhao C, Wang Z, Li Z, Kong X. Clinical diagnostic value of amino acids in laryngeal squamous cell carcinomas. PeerJ. 2023;11:e15469.
7. Zhong D, Wang Z, Ye Z, Wang Y, Cai X. Cancer-derived exosomes as novel biomarkers in metastatic gastrointestinal cancer. Mol Cancer. 2024;23(1):67.
8. Robbins J, Wakakuwa K, Ikeda H. Noradrenaline action on cat retinal ganglion cells is mediated by dopamine (D2) receptors. Brain Res. 1988;438(1–2):52–60.
9. Kalluri R. The biology and function of exosomes in cancer. J Clin Invest. 2016;126(4):1208–15.
10. Kobayashi H, Enomoto A, Woods SL, Burt AD, Takahashi M, Worthley DL. Cancer-associated fibroblasts in gastrointestinal cancer. Nat Rev Gastroenterol Hepatol. 2019;16(5):282–95.
11. Zhu L, Li J, Gong Y, Wu Q, Tan S, Sun D, et al. Exosomal tRNA-derived small RNA as a promising biomarker for cancer diagnosis. Mol Cancer. 2019;18(1):74.
12. Saadatpour L, Fadaee E, Fadaei S, Nassiri Mansour R, Mohammadi M, Mousavi SM, et al. Glioblastoma: exosome and microRNA as novel diagnosis biomarkers. Cancer Gene Ther. 2016;23(12):415–8.
13. Marin AM, Mattar SB, Amatuzzi RF, Chammas R, Uno M, Zanette DL, et al. Plasma Exosome-Derived microRNAs as Potential Diagnostic and Prognostic Biomarkers in Brazilian Pancreatic Cancer Patients. Biomolecules. 2022;12(6):769.
14. Gan Y, Kang Y, Zhong R, You J, Chen J, Li L, et al. Cancer testis antigen MAGEA3 in serum and serum-derived exosomes serves as a promising biomarker in lung adenocarcinoma. Sci Rep. 2024;14(1):7573.
15. Ohashi T, Terazawa K, Shibata H, Inoue N, Ogawa T. Metabolic profiling analysis of head and neck squamous cell carcinoma. Oral Dis. 2024;30(2):342–52.
16. DeFelice BC, Fiehn O, Belafsky P, Ditterich C, Moore M, Abouyared M, et al. Polyamine Metabolites as Biomarkers in Head and Neck Cancer Biofluids. Diagnostics (Basel). 2022;12(4):797.
17. Zhi Y, Wang Q, Zi M, Zhang S, Ge J, Liu K, et al. Spatial Transcriptomic and Metabolomic Landscapes of Oral Submucous Fibrosis-Derived Oral Squamous Cell Carcinoma and its Tumor Microenvironment. Adv Sci (Weinh). 2024;11(12):e2306515.
18. Blatt S, Voelxen N, Sagheb K, Pabst AM, Walenta S, Schroeder T, et al. Lactate as a predictive marker for tumor recurrence in patients with head and neck squamous cell carcinoma (HNSCC) post radiation: a prospective study over 15 years. Clin Oral Investig. 2016;20(8):2097–104.
19. Wu SL, Zha GY, Tian KB, Xu J, Cao MG. The metabolic reprogramming of γ-aminobutyrate in oral squamous cell carcinoma. BMC Oral Health. 2024;24(1):418.
20. Nicholson JK, Connelly J, Lindon JC, Holmes E. Metabonomics: a platform for studying drug toxicity and gene function. Nat Rev Drug Discov. 2002;1(2):153–61.
21. Wu H, Xue R, Tang Z, Deng C, Liu T, Zeng H, et al. Metabolomic investigation of gastric cancer tissue using gas chromatography/mass spectrometry. Anal Bioanal Chem. 2010;396(4):1385–95.
22. Huang Q, Tan Y, Yin P, Ye G, Gao P, Lu X, et al. Metabolic characterization of hepatocellular carcinoma using nontargeted tissue metabolomics. Cancer Res. 2013;73(16):4992–5002.
23. Ferrarini A, Di Poto C, He S, Tu C, Varghese RS, Kara Balla A, et al. Metabolomic Analysis of Liver Tissues for Characterization of Hepatocellular Carcinoma. J Proteome Res. 2019;18(8):3067–76.
24. Budczies J, Denkert C, Müller BM, Brockmöller SF, Klauschen F, Györffy B, et al. Remodeling of central metabolism in invasive breast cancer compared to normal breast tissue - a GC-TOFMS based metabolomics study. BMC Genomics. 2012;23(13):334.
25. Hori S, Nishiumi S, Kobayashi K, Shinohara M, Hatakeyama Y, Kotani Y, et al. A metabolomic approach to lung cancer. Lung Cancer. 2011;74(2):284–92.
26. Wojakowska A, Zebrowska A, Skowronek A, Rutkowski T, Polanski K, Widlak P, et al. Metabolic Profiles of Whole Serum and Serum-Derived Exosomes Are Different in Head and Neck Cancer Patients Treated by Radiotherapy. J Pers Med. 2020;10(4):229.
27. Huang Y, Liang J, Hu W, Liang Y, Xiao X, Zhao W, et al. Integration Profiling Between Plasma Lipidomics, Epstein-Barr Virus and Clinical Phenomes in Nasopharyngeal Carcinoma Patients. Front Microbiol. 2022;13:919496.
28. Tao L, Zhou J, Yuan C, Zhang L, Li D, Si D, et al. Metabolomics identifies serum and exosomes metabolite markers of pancreatic cancer. Metabolomics. 2019;15(6):86.
29. Zhu Q, Huang L, Yang Q, Ao Z, Yang R, Krzesniak J, et al. Metabolomic analysis of exosomal-markers in esophageal squamous cell carcinoma. Nanoscale. 2021;13(39):16457–64.
30. Hu S, Zhao C, Wang Z, Li Z, Kong X. Clinical diagnostic value of amino acids in laryngeal squamous cell carcinomas. PeerJ. 2023;11:e15469.
31. Huang CC, Tsai ST, Kuo CC, Chang JS, Jin YT, Chang JY, et al. Arginine deprivation as a new treatment strategy for head and neck cancer. Oral Oncol. 2012;48(12):1227–35.
32. Szefel J, Danielak A, Kruszewski WJ. Metabolic pathways of L-arginine and therapeutic consequences in tumors. Adv Med Sci. 2019;64(1):104–10.
33. Keibler MA, Wasylenko TM, Kelleher JK, Iliopoulos O, Vander Heiden MG, Stephanopoulos G. Metabolic requirements for cancer cell proliferation. Cancer Metab. 2016;4:16.

34. Johnson DE, Burtness B, Leemans CR, Lui VWY, Bauman JE, Grandis JR. Head and neck squamous cell carcinoma. Nat Rev Dis Primers. 2020;6(1):92.
35. Yu W, Hurley J, Roberts D, Chakrabortty SK, Enderle D, Noerholm M, et al. Exosome-based liquid biopsies in cancer: opportunities and challenges. Ann Oncol. 2021;32(4):466–77.
36. Cao J, Zhang M, Xie F, Lou J, Zhou X, Zhang L, et al. Exosomes in head and neck cancer: Roles, mechanisms and applications. Cancer Lett. 2020;1(494):7–16.
37. Zhao T, Liang Y, Zhen X, Wang H, Song L, Xing D, et al. Analysis of Serum Exosome Metabolites Identifies Potential Biomarkers for Human Hepatocellular Carcinoma. Metabolites. 2024;14(8):462.
38. Cheng L, Zhang K, Qing Y, Li D, Cui M, Jin P, et al. Proteomic and lipidomic analysis of exosomes derived from ovarian cancer cells and ovarian surface epithelial cells. J Ovarian Res. 2020;13(1):9.
39. Brzozowski JS, Jankowski H, Bond DR, McCague SB, Munro BR, Predebon MJ, et al. Lipidomic profiling of extracellular vesicles derived from prostate and prostate cancer cell lines. Lipids Health Dis. 2018;17(1):211.
40. Bestard-Escalas J, Reigada R, Reyes J, de la Torre P, Liebisch G, Barceló-Coblijn G. Fatty Acid Unsaturation Degree of Plasma Exosomes in Colorectal Cancer Patients: A Promising Biomarker. Int J Mol Sci. 2021;22(10):5060.
41. Cao Y, Qin Y, Cheng Q, Zhong J, Han B, Li Y. Bifunctional nanomaterial enabled high-specific isolation of urinary exosomes for cervical cancer metabolomics analysis and biomarker discovery. Talanta. 2025;1(285):127280.
42. Nishida-Aoki N, Izumi Y, Takeda H, Takahashi M, Ochiya T, Bamba T. Lipidomic Analysis of Cells and Extracellular Vesicles from High- and Low-Metastatic Triple-Negative Breast Cancer. Metabolites. 2020;10(2):67.
43. Castellanos-Rizaldos E, Zhang X, Tadigotla VR, Grimm DG, Karlovich C, Raez LE, et al. Exosome-based detection of activating and resistance EGFR mutations from plasma of non-small cell lung cancer patients. Oncotarget. 2019;10(30):2911–20.
44. McKiernan J, Donovan MJ, O'Neill V, Bentink S, Noerholm M, Belzer S, et al. A Novel Urine Exosome Gene Expression Assay to Predict High-grade Prostate Cancer at Initial Biopsy. JAMA Oncol. 2016;2(7):882–9.
45. Yuan Q, Yin L, He J, Zeng Q, Liang Y, Shen Y, et al. Metabolism of asparagine in the physiological state and cancer. Cell Commun Signal. 2024;22(1):163.
46. Albert AE, Adua SJ, Cai WL, Arnal-Estapé A, Cline GW, Liu Z, et al. Adaptive Protein Translation by the Integrated Stress Response Maintains the Proliferative and Migratory Capacity of Lung Adenocarcinoma Cells. Mol Cancer Res. 2019;17(12):2343–55.
47. Patil MD, Bhaumik J, Babykutty S, Banerjee UC, Fukumura D. Arginine dependence of tumor cells: targeting a chink in cancer's armor. Oncogene. 2016;35(38):4957–72.
48. Khadeir R, Szyszko T, Szlosarek PW. Optimizing arginine deprivation for hard-to-treat cancers. Oncotarget. 2017;8(57):96468–9.
49. Pegg AE. Functions of Polyamines in Mammals. J Biol Chem. 2016;291(29):14904–12.
50. Lee CY, Su GC, Huang WY, Ko MY, Yeh HY, Chang GD, et al. Promotion of homology-directed DNA repair by polyamines. Nat Commun. 2019;10(1):65.
51. Carrer A, Trefely S, Zhao S, Campbell SL, Norgard RJ, Schultz KC, et al. Acetyl-CoA Metabolism Supports Multistep Pancreatic Tumorigenesis. Cancer Discov. 2019;9(3):416–35.
52. Li J, Li J, Wang H, Qi LW, Zhu Y, Lai M. Tyrosine and Glutamine-Leucine Are Metabolic Markers of Early-Stage Colorectal Cancers. Gastroenterology. 2019;157(1):257-259.e5.
53. Hershberger CE, Rodarte AI, Siddiqi S, Moro A, Acevedo-Moreno LA, Brown JM, et al. Salivary Metabolites are Promising Non-Invasive Biomarkers of Hepatocellular Carcinoma and Chronic Liver Disease. Liver Cancer Int. 2021;2(2):33–44.
54. Somashekar BS, Kamarajan P, Danciu T, Kapila YL, Chinnaiyan AM, Rajendiran TM, et al. Magic angle spinning NMR-based metabolic profiling of head and neck squamous cell carcinoma tissues. J Proteome Res. 2011;10(11):5232–41.
55. Neurauter G, Grahmann AV, Klieber M, Zeimet A, Ledochowski M, Sperner-Unterweger B, et al. Serum phenylalanine concentrations in patients with ovarian carcinoma correlate with concentrations of immune activation markers and of isoprostane-8. Cancer Lett. 2008;272(1):141–7.
56. Wiggins T, Kumar S, Markar SR, Antonowicz S, Hanna GB. Tyrosine, phenylalanine, and tryptophan in gastroesophageal malignancy: a systematic review. Cancer Epidemiol Biomarkers Prev. 2015;24(1):32–8.
57. Jobard E, Pontoizeau C, Blaise BJ, Bachelot T, Elena-Herrmann B, Trédan O. A serum nuclear magnetic resonance-based metabolomic signature of advanced metastatic human breast cancer. Cancer Lett. 2014;343(1):33–41.
58. Li J, Liu K, Ji Z, Wang Y, Yin T, Long T, et al. Serum untargeted metabolomics reveal metabolic alteration of non-small cell lung cancer and refine disease detection. Cancer Sci. 2023;114(2):680–9.
59. Casals N, Zammit V, Herrero L, Fadó R, Rodríguez-Rodríguez R, Serra D. Carnitine palmitoyltransferase 1C: From cognition to cancer. Prog Lipid Res. 2016;61:134–48.
60. Indiveri C, Iacobazzi V, Tonazzi A, Giangregorio N, Infantino V, Convertini P, et al. The mitochondrial carnitine/acylcarnitine carrier: Function, structure and physiopathology. Mol Aspects Med. 2011;32(4):223–33.
61. Gerner EW, Meyskens FL. Polyamines and cancer: old molecules, new understanding. Nat Rev Cancer. 2004;4(10):781–92.
62. Holbert CE, Cullen MT, Casero RA, Stewart TM. Polyamines in cancer: integrating organismal metabolism and antitumour immunity. Nat Rev Cancer. 2022;22(8):467–80.
63. Xu H, Liu R, He B, Bi CW, Bi K, Li Q. Polyamine Metabolites Profiling for Characterization of Lung and Liver Cancer Using an LC-Tandem MS Method with Multiple Statistical Data Mining Strategies: Discovering Potential Cancer Biomarkers in Human Plasma and Urine. Molecules. 2016;21(8):1040.
64. Tse RTH, Wong CYP, Chiu PKF, Ng CF. The Potential Role of Spermine and Its Acetylated Derivative in Human Malignancies. Int J Mol Sci. 2022;23(3):1258.
65. Al-Habsi M, Chamoto K, Matsumoto K, Nomura N, Zhang B, Sugiura Y, et al. Spermidine activates mitochondrial trifunctional protein and improves antitumor immunity in mice. Science (New York, NY) [Internet]. 2022;378(6618). [cited 2024 Sep 18]. Available from: https://pubmed.ncbi.nlm.nih.gov/36302005/.
66. Liu G, Xu X, Wu C, Jia G, Zhao H, Chen X, et al. Spermine protects intestinal barrier integrity through ras-related C3 botulinum toxin substrate 1/phospholipase C-γ1 signaling pathway in piglets. Anim Nutr. 2021;13(8):135–43.
67. Guo Y, Ye Q, Deng P, Cao Y, He D, Zhou Z, et al. Spermine synthase and MYC cooperate to maintain colorectal cancer cell survival by repressing Bim expression. Nat Commun. 2020;11(1):3243.
68. Guo Z, Zhang X, Lin C, Huang Y, Zhong Y, Guo H, et al. METTL3-IGF2BP3-axis mediates the proliferation and migration of pancreatic cancer by regulating spermine synthase m6A modification. Front Oncol. 2022;12:962204.
69. Shukla-Dave A, Hricak H, Moskowitz C, Ishill N, Akin O, Kuroiwa K, et al. Detection of prostate cancer with MR spectroscopic imaging: an expanded paradigm incorporating polyamines. Radiology. 2007;245(2):499–506.
70. Li X, Li F, Ye F, Guo H, Chen W, Jin J, et al. Spermine is a natural suppressor of AR signaling in castration-resistant prostate cancer. Cell Rep. 2023;42(7):112798.
71. Harrison GA. Spermine in human tissues. Biochem J. 1931;25(6):1885–92.
72. Sun Y, Zhou P, Qian J, Zeng Q, Wei G, Li Y, et al. Spermine synthase engages in macrophages M2 polarization to sabotage antitumor immunity in hepatocellular carcinoma. Cell Death Differ. 2024. https://doi.org/10.1038/s41418-024-01409-z.
73. Xu H, Zhang X, Wang X, Li B, Yu H, Quan Y, et al. Cellular spermine targets JAK signaling to restrain cytokine-mediated autoimmunity. Immunity. 2024;57(8):1796-1811.e8.
74. Gong W, Donnelly CR, Heath BR, Bellile E, Donnelly LA, Taner HF, et al. Cancer-specific type-I interferon receptor signaling promotes cancer stemness and effector CD8+ T-cell exhaustion. Oncoimmunology. 2021;10(1):1997385.
75. Pan X, Xue L, Sun Y. Spermine synthase (SMS) serves as a prognostic biomarker in head and neck squamous cell carcinoma: a bioinformatics analysis. Ann Transl Med. 2022;10(22):1213.
76. Wu M, Xu Y, Fitch WL, Zheng M, Merritt RE, Shrager JB, et al. Liquid chromatography/mass spectrometry methods for measuring dipeptide

abundance in non-small-cell lung cancer. Rapid Commun Mass Spectrom. 2013;27(18):2091–8.
77. Oksvold MP, Neurauter A, Pedersen KW. Magnetic bead-based isolation of exosomes. Methods Mol Biol. 2015;1218:465–81.
78. Tauro BJ, Greening DW, Mathias RA, Mathivanan S, Ji H, Simpson RJ. Two distinct populations of exosomes are released from LIM1863 colon carcinoma cell-derived organoids. Mol Cell Proteomics. 2013;12(3):587–98.
79. Laulagnier K, Motta C, Hamdi S, Roy S, Fauvelle F, Pageaux JF, et al. Mast cell- and dendritic cell-derived exosomes display a specific lipid composition and an unusual membrane organization. Biochem J. 2004;380(Pt 1):161–71.

Publisher's Note